

Search for Higgs Boson at LHC in the Reaction $pp \rightarrow \gamma\gamma + jet$ at a Low Luminosity *

M.N. Dubinin, V.A. Ilyin and V.I. Savrin

Institute of Nuclear Physics, Moscow State University, 119899 Moscow, Russia

Abstract

We discuss the SM Higgs discovery potential of the LHC in the channel $pp \rightarrow H + jet \rightarrow \gamma\gamma + jet$ when the jet is observed at sufficiently high p_t and a small rapidity to be reliably identified. We calculate all the signal subprocesses and the irreducible background with realistic kinematical cuts. The reducible QCD background is also estimated.

We conclude that the channel $\gamma\gamma + jet$ can give about 120-200 signal events for Higgs mass $M_H = 100-140$ GeV at the integrated luminosity of 30fb^{-1} . This signal rate should be compared with only $\sim 330-600$ events for the irreducible background per two-photon invariant mass interval of 2 GeV. We estimate the QCD reducible background at the level of $\leq 20\%$ of the irreducible one. Thus, one may hope that the Higgs boson can be discovered already during the LHC operation at a low luminosity. At a high luminosity of $10^{34} \text{ cm}^{-2}\text{s}^{-1}$ the observation of several hundreds of high p_t Higgs bosons in this channel will be possible with significance higher than 15 for $L \sim 100\text{fb}^{-1}$.

1 Introduction

It is well known that the observation of a light Higgs boson ($M_H < 140$ GeV) at the LHC collider in the inclusive channel $pp \rightarrow \gamma\gamma + X$ is not easy [2, 3, 4]. Even if we can reduce the misidentification of two jets as photons to a small level, the irreducible background from the $q\bar{q} \rightarrow \gamma\gamma$ and $gg \rightarrow \gamma\gamma$ subprocesses rapidly increases for smaller $\gamma\gamma$ pair invariant masses, and it is necessary to separate a rather elusive Higgs boson signal from it. In this situation it is important to understand whether we can observe at the LHC any other Higgs boson production mechanisms. In this paper we are considering the Higgs discovery potential in the channel $pp \rightarrow \gamma\gamma + jet$ when the jet is observed at a sufficiently high transverse momentum and small rapidity to be reliably identified. In this channel the signal cross section is much smaller in comparison with the inclusive $pp \rightarrow \gamma\gamma + X$ case, but at the same time the situation with the background is undoubtedly much better. Transition to larger p_t allows us to reduce the overwhelming backgrounds of the completely inclusive channel mentioned above. We consider the scalar boson production in the framework of Standard Model (SM) with one Higgs doublet.

The idea to look for the Higgs boson signal associated with a high p_t jet in the final state was considered in [5], where the matrix elements of signal subprocesses $gg \rightarrow g + H$, $gq \rightarrow q + H$ and $q\bar{q} \rightarrow g + H$ were calculated analytically in the leading order α_s^3 . In [6] the corresponding subprocesses were calculated for the case of CP-odd Higgs boson production within the minimal supersymmetric extension of the Standard Model (MSSM). Recently (see Ref. [7]) the matrix elements for subprocesses $gq \rightarrow H^\pm q', H_i^0 q$ were calculated analytically for charged and neutral scalars in the framework of MSSM. However, in [6, 7] decay channels of the Higgs were not considered and in [5] only the final state $\tau^+ \tau^- + jet$ was discussed. In [8] the SM subprocesses were considered for the case of heavy Higgs boson decaying into the WW or ZZ pairs. Very promising numbers have been obtained recently in [9] for $\gamma\gamma + 2jets$ final state with two very forward jets ($|\eta_{jet}| < 5$), when Higgs scalars are produced by weak boson fusion mechanism. In this reaction 10-20 Higgs signal events could be observed with the significance equal to 3.5-7 at the integrated luminosity 10 fb^{-1} . In [10] (see also [3]) the final state $\gamma\gamma + (\geq 2jets)$ was simulated by means of PYTHIA generator [11] in the realistic CMS detector environment. The events with relatively small

*To appear in: *Proceedings of XIIth International Workshop: High Energy Physics and Quantum Field Theory (QFTHEP-97)*, Samara, Russia, September 4-10, 1997. Preliminary version of this paper was included in [1], where we studied also the possibilities of Higgs signal observation in the final state $\gamma\gamma + lepton$ for the LHC high luminosity regime.

rapidity jets and the events with very forward jets, produced by weak boson fusion mechanism, were studied there (as we mentioned above, independent analysis of the fusion can be found in [9]). It was shown that this signature has good prospects for the light Higgs boson search giving $\sim 100\text{-}150$ signal events at the integrated luminosity of 160 fb^{-1} (about one and a half year of LHC operation at the high luminosity of $10^{34}\text{cm}^{-2}\text{s}^{-1}$) with approximately the same number of background events.

The final state $\gamma\gamma + jet$, with high p_t and small rapidity jet recoiling against the Higgs boson, has not been analysed and we discuss it in detail in Section 4. The possibility of charged particle tracks reconstruction in the central detector is an advantage of this signature ($E_t^{jet} > 40\text{ GeV}$ and $|\eta_{jet}| < 2.4$). Final state jet reconstruction allows to determine more precisely the position of interaction vertex, thus giving the possibilities to improve two photon invariant mass resolution. This point could be important for the separation of reducible QCD background. We calculate all the signal subprocesses and the irreducible background applying realistic kinematical cuts. The reducible QCD background is estimated as well.

We calculated cross sections and distributions with the help of CompHEP package [12, 13]. Exact one-loop matrix elements for the signal QCD subprocesses were implemented in the CompHEP FORTRAN output, thus we got a possibility to use CompHEP numerical module for integration over the phase space. Then, the vertex ggH in the signal QCD diagrams, including quark loops, was implemented in CompHEP as an effective point-like vertex together with the $gggH$ vertex to ensure gauge invariance of the amplitude. Thus we tested an accuracy of the effective Lagrangian approximation.

The CompHEP package includes the code of adaptive MC integrator VEGAS [14]. For parton distribution functions we used the parametrizations CTEQ3m [15], CTEQ4m and CTEQ4l [16], MRS-A' [17] and GRV92 (HO) [18]. The corresponding codes are also implemented in CompHEP.

The paper is organized as follows. In Section 2 we list the values of physical parameters and some physical conventions.

In Section 3 we discuss basic formulas for the $H \rightarrow \gamma\gamma$ branching and the ggH vertex. To test the code written by using these basic formulas we compare results obtained by means of CompHEP, PYTHIA 6.1 [11] and the programs HDECAY/HIGLU [19] for $H \rightarrow \gamma\gamma$ and for the reaction $pp \rightarrow H \rightarrow \gamma\gamma$.

In Section 4 we analyse the reaction $pp \rightarrow \gamma\gamma + jet$. In Section 4.1 the signal QCD subprocesses $gg \rightarrow H + g$, $gq \rightarrow H + q$ and $q\bar{q} \rightarrow H + g$ are discussed. The corresponding formulas for their matrix elements in the limit of heavy t -quark mass are given, what turns out to be a precise enough approximation. Detailed analysis of the main signal and background subprocesses, $gg \rightarrow H + g \rightarrow \gamma\gamma + g$ and $gq \rightarrow \gamma + \gamma + q$, is presented in Section 4.2. We introduce different cuts looking for the possibilities to get a better significance of the Higgs signal in the $\gamma\gamma + jet$ final state. In Section 4.3 the contributions of all signal and irreducible background subprocesses are discussed. Then, in Section 4.4, we estimate the QCD reducible background. In Section 4.5 a general discussion for the reaction $pp \rightarrow \gamma\gamma + jet$ is given.

In Conclusion the prospects to search for the light Higgs boson at low LHC luminosity are summarised.

2 Input parameters and physical conventions

In our calculations we used $\sqrt{s} = 14\text{ TeV}$ and $M_Z = 91.1884\text{ GeV}$, $\sin^2 \theta_w = 0.2237$. For heavy quark masses we took the values $m_s = 0.2\text{ GeV}$, $m_c = 1.3\text{ GeV}$, $m_b = 4.3\text{ GeV}$ and $m_t = 175\text{ GeV}$ [20]¹.

Most of the hard subprocesses that we are discussing involve QCD vertices. For the strong coupling constant we are using the normalization

$$\alpha_s(M_Z) = 0.118,$$

where α_s runs in correspondence with the 2nd order QCD (NLO) formulas with flavour matching (see, e.g., [20], p.77). This normalization assumes that $\Lambda_{QCD}^{(5)} = 226\text{ MeV}$. For instance, $\alpha_s(120\text{GeV}) = 0.1133$.

In electroweak vertices we used $\alpha(M_Z) = 1/128.9$ [20] calculating electroweak couplings and the Fermi constant by means of the corresponding formulas with $\alpha(M_Z)$, M_Z and $\sin^2 \theta_w$ as independent parameters. However, it is more accurate to use $\alpha(m_e) = 1/137.036$ in each vertex that includes an on-shell photon because of the absence of photon wave function renormalization in this case. Thus we introduce the correction factor $(128.9/137.036)^2$ for each process with two photons in the final state.

¹We shall not discuss the sensitivity of our results to the value of t -quark mass. Recent CDF/D0 data gives $m_t = 175.6 \pm 5.5\text{ GeV}$ [21]. Rather small uncertainty of m_t does not change significantly cross sections of the processes under consideration.

3 Higgs decays and the effective Lagrangian

It is well known that in the case when $M_H < 140$ GeV the Higgs boson decays dominantly into a $b\bar{b}$ pair. However, the QCD corrections to this decay partial width are large. So, for reactions where the $H \rightarrow \gamma\gamma$ decay occurs it is important to take into account carefully these corrections because they increase the two-photon branching approximately by a factor of 2. In this section we also discuss all other decay channels related to the $H \rightarrow \gamma\gamma$ branching and the effective $\gamma\gamma H$ Lagrangian which can be used for calculation of the partial width $\Gamma_{H \rightarrow \gamma\gamma}$. Similar effective ggH Lagrangian can be used in calculation of the partial width of Higgs decay into a gluon pair and the cross sections of signal QCD processes.

In order to take into account the QCD corrections the NNLO formulas improved by the renormalization group method [22] were proposed for the running quark masses. We implemented in CompHEP the corresponding NLO formulas for the Higgs decay into quarks. This approximation gives results for partial widths higher than the NNLO formulas by $\sim 10\%$ and the corresponding correction factor has been introduced in our computer code.

Electroweak corrections to the Higgs decays into quarks and leptons are small [23] and we neglect them.

Analytical formulas for the partial widths $\Gamma_{H \rightarrow \gamma\gamma}$ and $\Gamma_{H \rightarrow gg}$ in the leading one-loop approximation are known for many years [24]. They can be obtained with the help of the following effective Lagrangians:

$$\begin{aligned}\mathcal{L}_{\gamma\gamma H}^{eff} &= \frac{\lambda_{\gamma\gamma H}}{2} F_{\mu\nu} F^{\mu\nu} H, \\ \mathcal{L}_{ggH}^{eff} &= K \frac{\lambda_{ggH}}{2} G_{\mu\nu}^a G^{a\mu\nu} H.\end{aligned}\quad (1)$$

Here $F_{\mu\nu}$ and $G_{\mu\nu}^a$ are photon and gluon field strengths, correspondingly, and K is a factor accounting for high order QCD corrections. Analytical formulas for the effective coupling constants $\lambda_{\gamma\gamma H}$ and λ_{ggH} in the leading order approximation can be found in Refs. [24]. The corresponding partial widths are

$$\Gamma_{H \rightarrow \gamma\gamma} = \frac{\lambda_{\gamma\gamma H}^2}{16\pi} \cdot M_H^3, \quad \Gamma_{H \rightarrow gg} = K^2 \cdot \frac{\lambda_{ggH}^2}{2\pi} \cdot M_H^3.$$

Total QCD radiative corrections to the $H \rightarrow gg$ partial width can be collected in a factor with value ~ 1.7 [25, 26, 27, 28]. Note that the QCD radiative corrections to the partial width of $H \rightarrow \gamma\gamma$ are very small (less than 1%, see, e.g. [27] and references therein).

Electroweak corrections to the partial widths of $H \rightarrow \gamma\gamma$ and $H \rightarrow gg$ are small and can be neglected [29].

In the limit $m_t \rightarrow \infty$ and without contributions from the light quark loops the ggH effective coupling constant has a very simple form

$$\lambda_{ggH} \Big|_{m_t \rightarrow \infty} = \frac{\alpha_s g_w}{12\pi M_W}, \quad (2)$$

where the electroweak constant is $\alpha_w = g_w^2/4\pi = \alpha(M_Z)/\sin^2\theta_w$. As we shall see the effective Lagrangian (1) with the coupling constant (2) can be used in calculations of the signal subprocesses with acceptable accuracy.

We remark that for a precise calculation of the $H \rightarrow \gamma\gamma$ branching in the Higgs mass range considered one has to account also for the partial width $\Gamma_{H \rightarrow WW^*}$, where W^* means the off-shell W -boson. At the mass values close to $M_H = 140$ GeV this branching and the branching to a $b\bar{b}$ pair are of the same order. The corresponding analytical formulas can be found in [31].

All formulas for the partial widths mentioned above and the higher order QCD correction factors were implemented in the CompHEP codes. We checked the numbers obtained for the branching $H \rightarrow \gamma\gamma$ by means of CompHEP, PYTHIA 6.1 and the program HDECAY [19]:

M_H GeV	$Br(H \rightarrow \gamma\gamma) \cdot 10^{-3}$		
	CompHEP	HDECAY	PYTHIA
100	1.999	1.961	2.065
120	2.723	2.707	2.857
140	2.148	2.151	2.327

One can see a good agreement of our numbers with the results of the HDECAY program (where all known formulas for higher order corrections are used). At the same time one can see that the PYTHIA results are 5-8% higher.

To test our code written for the effective coupling constant λ_{ggH} (in leading order) we compared also the numbers obtained for the $pp \rightarrow H \rightarrow \gamma\gamma$ cross section by means of CompHEP, PYTHIA 6.1 and HIGLU/HDECAY programs:

package	PDF set	$\sigma^{tot}(gg \rightarrow H \rightarrow \gamma\gamma)$, fb		
		$M_H = 100$ GeV	120 GeV	140 GeV
CompHEP	CTEQ3m	37.18	41.03	26.85
	GRV92(HO)	38.08	41.11	26.45
HIGLU/HDECAY	GRV92(HO)	39.59	40.78	25.17
PYTHIA 6.1	CTEQ3m	38.96	40.97	26.65

Here we used $Q^2 = M_H^2$ for the parton factorization scale. The strong coupling was taken fixed at the value of Higgs mass. The hard subprocess $gg \rightarrow H$ was calculated in leading order α_s^2 . Values of the $H \rightarrow \gamma\gamma$ branching used in these programs are given above. One can see that all three programs are in agreement with each other within 5%.

4 Higgs boson signal in the reaction $pp \rightarrow \gamma\gamma + jet$

In this section we study systematically processes with the final state $\gamma\gamma + jet$.

First of all let us note that the signal subprocesses contributing to this reaction are QCD subprocesses, and it means that the cross sections should depend strongly on QCD parameters. There are three main sources of this dependence. The first one is defined by the evolution of the parton densities. Then, the hard subprocess cross sections depend on the running α_s . Finally, the $H \rightarrow \gamma\gamma$ branching depends on the Higgs total width, where the QCD corrections are large (see a short discussion in Section 3 and the corresponding references). In leading order all these three sources can be factorized. Moreover, due to a very small value of Γ_H^{tot} in the Higgs mass range of 100-140 GeV the decay width of $H \rightarrow \gamma\gamma$ can be factorized, and the fixed value of strong coupling $\alpha_s(M_H)$ can be used for evaluation of the $H \rightarrow \gamma\gamma$ branching. However, it is well-known that for the reaction $pp \rightarrow H \rightarrow \gamma\gamma$ the dependence on the QCD normalization scale μ (used in calculations of the QCD corrections to hard subprocesses) and on the parton factorization scale Q is strong enough and next-to-leading analysis is necessary (see, e.g. [27] and references therein). For the reaction $pp \rightarrow H \rightarrow \gamma\gamma$ after including the NLO corrections, this theoretical uncertainty decreases considerably, showing only a $\sim 15\%$ remaining (μ, Q) sensitivity. Surely one can expect a similar effect also for the Higgs production at high p_t . The self-consistent analysis requires the NLO corrections to hard subprocesses which are not known yet. Thus, today we cannot analyse the reaction $pp \rightarrow \gamma\gamma + jet$ in the complete NLO approximation. Therefore, in this paper some kind of combined accounting for the QCD effects is used: NLO PDF evolution and LO approximation for hard subprocesses (but with NLO running α_s).

4.1 Signal QCD subprocesses

There are three hard QCD subprocesses with a signal from the Higgs boson contributing to the reaction $pp \rightarrow \gamma\gamma + jet$:

$$gg \rightarrow H + g, \quad gq \rightarrow H + q, \quad q\bar{q} \rightarrow H + g. \quad (3)$$

In Fig. 1 Feynman diagrams contributing in leading order α_s^3 are shown. Here the vertices ggH and $gggH$ are substituted instead of the corresponding vertices with quark loops in exact calculations and represent the effective point-like vertices of the Lagrangian (1,2) in the approximate calculations.

The corresponding matrix elements were calculated analytically in [5]. In the limit $m_t \rightarrow \infty$ the differential cross sections are

$$\frac{d\sigma_{gg}}{d\hat{t}} \Big|_{m_t \rightarrow \infty} = \frac{1}{16\pi s^2} \cdot \frac{\alpha_w \alpha_s^3}{24} \left[\frac{M_H^8 + \hat{s}^4 + \hat{t}^4 + \hat{u}^4}{\hat{s}\hat{t}\hat{u}M_W^2} \right], \quad (4)$$

$$\frac{d\sigma_{gq}}{d\hat{t}} \Big|_{m_t \rightarrow \infty} = \frac{1}{16\pi s^2} \cdot \frac{\alpha_w \alpha_s^3}{54} \cdot \frac{\hat{s}^2 + \hat{u}^2}{(-\hat{t}) M_W^2}, \quad \frac{d\sigma_{q\bar{q}}}{d\hat{t}} \Big|_{m_t \rightarrow \infty} = \frac{1}{16\pi s^2} \cdot \frac{4\alpha_w \alpha_s^3}{81} \cdot \frac{\hat{t}^2 + \hat{u}^2}{\hat{s} M_W^2}.$$

Here \hat{s} , \hat{t} and \hat{u} are the standard Mandelstam variables for partons in their c.m. system. These formulas can be derived from the effective Lagrangian (1), (2).

We found that the approximation (4) works well enough. For the channel gg this approximation gives numbers slightly smaller than the exact matrix elements – the difference is less than 7% at the transverse momentum cut $p_t > 40$ GeV and $|\eta_{jet}| < 2.4$. For the channel gq this approximation overestimates the exact result by $\sim 13\%$ with the same cuts. For the channel $q\bar{q}$ the approximation (4) does not work at all, however, the contribution of this channel to the process $pp \rightarrow \gamma\gamma + jet$ is much smaller than the contribution of gg and gq channels and can be neglected. Thus, the precision of the effective Lagrangian approximation in calculation of the QCD signal processes (3) is better than 7%. This fact allows in principle to create a fast generator of signal events for the reaction $pp \rightarrow \gamma\gamma + jet$. Detailed analysis of the approximation [3] will be published elsewhere [32].

We checked that the PYTHIA result is also in good agreement with exact calculations, giving cross section higher by $\sim 6\%$.

4.2 $pp \rightarrow H + g \rightarrow \gamma\gamma + g$ versus $pp \rightarrow \gamma + \gamma + q$

In this section we consider the contribution of the signal subprocess $gg \rightarrow H + g \rightarrow \gamma\gamma + g$ (four diagrams in Fig.1a). We compare the corresponding cross section and distributions with those of the background $gq \rightarrow \gamma + \gamma + q$ subprocess, $q = u, d$. Tree level Feynman diagrams contributing to this background are shown in Fig. 3a. Let us stress that the two subprocesses considered give the main contributions to the signal and background. In this section we look for the possibilities to get a better significance of the Higgs signal varying the cuts on different variables.

In the following we consider realistic cuts [3, 4] for the final state $\gamma\gamma + jet$ (which we shall refer as to the **(C)** set of cuts):²

- (C1) two photons are required with $p_t^\gamma > 40$ GeV and $|\eta_\gamma| < 2.5$ for each photon;
- (C2) photons are isolated from each other by $\Delta R(\gamma_1, \gamma_2) > 0.3$;
- (C3) jet has high transverse energy $E_t^{jet} > 40$ GeV and is centrally produced, $|\eta_{jet}| < 2.4$;
- (C4) jet is isolated from the photons by $\Delta R(jet, \gamma_1) > 0.3$ and $\Delta R(jet, \gamma_2) > 0.3$.

In the following we shall vary the value of the kinematical cut on one of the variables starting from this basic set and leave a more tuned multivariable analysis for the future.

It is clear that the signal significance depends strongly on the two-photon invariant mass resolution. This key instrumental characteristic at a low luminosity is expected to be ~ 1.3 GeV for the CMS electromagnetic calorimeter [3] and ~ 3.1 GeV for the ATLAS calorimeter [4] ($M_H = 100$ GeV). These numbers are for the case of $\sim 80\%$ signal events reconstruction. Hereafter we shall integrate the background over $\gamma\gamma$ invariant mass within the range $M_H - \Delta M_{\gamma\gamma} < M_{\gamma\gamma} < M_H + \Delta M_{\gamma\gamma}$ with $\Delta M_{\gamma\gamma} = 1$ GeV.

Cross sections of the subprocesses under discussion convoluted with various parametrizations of the parton distributions for the basic set of kinematical cuts (**C**) and for $M_H = 120$ GeV are

	CTEQ4m	CTEQ3m	MRS-A'
(S) , fb	4.32	4.65	4.44
(B)/2GeV , fb	11.89	11.94	11.94

Thereinafter we denote by **(S)** the signal process $pp \rightarrow H + g \rightarrow \gamma\gamma + g$ and by **(B)** the background process $pp \rightarrow \gamma + \gamma + q$. Here we use $Q^2 = M_H^2 + 2(E_t^{jet})^2$ as the parton factorization scale.

To estimate the NLO corrections we calculated these cross sections also with the leading order parametrization CTEQ4l and with strong coupling running in leading order. The LO results appear to be $\sim 15\%$ lower for the signal and only $\sim 3\%$ lower for the background. For the signal about 2/3 of

² $\Delta R = \sqrt{\Delta\eta^2 + \Delta\phi^2}$ is a separation between two particles in the *azimuth angle – rapidity* plane.

this difference is due to the running of α_s , while for the background practically all the decrease is related to the PDF evolution.

The parton c.m. energy distributions presented in Fig. 4 show that almost all events have a small parton c.m. energies $\sqrt{\hat{s}} \leq 300$ GeV. So the phase space region for the process under discussion is characterized by the relations $\sqrt{\hat{s}} \sim M_H \sim m_t$. It means that we have events with very small values of the Bjorken variable $x \sim 3 \cdot 10^{-4}$. For these small x values the recent DIS data from HERA [30] show some discrepancy with the existing parametrizations, especially for the gluon distribution. This data, as well as the recent DIS data from the NMC and E665 experiments and from precision measurements of the inclusive jet production at Tevatron, were used to improve the parton distributions by the CTEQ Collaboration [16]. We have found that its latest parametrization CTEQ4m gives results lower than the previous set CTEQ3m by $\sim 7.5\%$ for the signal and only by $\sim 0.5\%$ for the background subprocesses (see the Table above). We use the CTEQ4m parametrization ($\alpha_s(M_Z) = 0.116$, $\Lambda_{QCD}^{(5)} = 202$ MeV) in our calculations. Furthermore, we calculated the cross sections with different choices of the Q^2 parameter which was used for both the parton factorization scale and the normalization for running α_s (numbers in the Table below are for $M_H = 120$ GeV):

	$Q^2 = M_H^2 + 2(E_t^{jet})^2$	M_H^2	$(E_t^{jet})^2$
(S) , fb	4.32	4.99	5.73
(B) / 2GeV , fb	11.89	12.18	12.68

One can see a much stronger dependence on the choice of QCD parameter Q^2 for the signal cross sections than for the background ones. Of course, it is caused by higher QCD order (α_s^3) of the signal subprocesses, while the background is only of order of α_s . In the following we use $Q^2 = M_H^2 + 2(E_t^{jet})^2$ which is intuitively more relevant to physics discussed here.

Let us look at the rapidity interval between the jet and the Higgs boson due to which the minijet corrections [33] could give some enhancement factor if one considers the semi-inclusive process $pp \rightarrow H + jet + X$. In Fig. 5 the distribution in the rapidity interval ($y_{jet} - y_H$) is presented. One can see that this interval is less than ± 3 . So the corresponding minijet corrections should be small unlike in the case of SSC discussed in [33].

Then, in Fig. 6 one can see that varying the cuts on photon rapidities around set (C) values does not help to improve signal significance. However, a change of the jet rapidity acceptance does show some prospects (Fig. 7). In Table 1(a)³ one can see that the significance increases when the jets with larger rapidities are detected. For example, we get a $\sim 14\%$ increase of significance if the $|\eta^j| < 2.4$ cut is replaced by $|\eta^j| < 4$ with involving the very forward hadron calorimeter.

The distribution in the jet transverse energy for the two processes discussed are shown in Fig. 8 for two values of the photon transverse momentum cut $p_t^\gamma > 20$ and 40 GeV. One can see that the application of a stronger cut improves the S/B ratio. This ratio increases also for a stronger E_t^{jet} cut (see Fig. 9).⁴ Let us see, however, what significance do we have. We have found that the variation of p_t^γ around set (C) values does not help to improve it. However, the application of a weaker cut on the analogous jet variable E_t^{jet} does improve the signal significance. For example, a replacement of the cut $E_t^{jet} > 40$ GeV by $E_t^{jet} > 30$ GeV increases the significance by $\sim 8\%$ but leads to a small decrease of the ratio S/B , see Table 1(b).

We analysed also a variety of other cuts, in particular, the cuts on transverse momenta of the photons, their relative angle in the two-photon rest frame and their separation cut. We treated also the cut on photon pair transverse momentum $p_t^{\gamma_1 + \gamma_2}$, and different cuts related to the planarity features of events. Unfortunately these variables did not show any possibilities to get a better signal significance.

4.3 Other signal and (irreducible) background processes

A number of other subprocesses contribute to the reaction $pp \rightarrow \gamma\gamma + jet$, both to the signal and background. We have calculated all of them within the framework described above. Results are collected in Table 2.

³Here the *effective* significance $\sigma_S/\sqrt{\sigma_B}$ is presented rather than usually used $N_S/\sqrt{N_B}$. To get the latter one should multiply the effective significance by the square root of the integrated luminosity.

⁴Some suppression in the interval $(M_H - \bar{E}_t^{jet})/2 < p_t^\gamma < (M_H + \bar{E}_t^{jet})/2$ is connected with the cut applied on the jet transverse energy $E_t^{jet} > \bar{E}_t^{jet}$.

Signal subprocesses can be subdivided in two groups. In the first group there are QCD subprocesses (3) discussed in Section 4.1. Numerically the gq channels give about 12% of the main gg signal contribution, while the $q\bar{q}$ channels can be neglected.

The second group of signal subprocesses is made up of electroweak reactions with Higgs production through WW or ZZ fusion, where one spectator quark produces the jet with high E_t . Of course, if one discusses the signature with only one jet one should assume that the set of kinematical cuts applied by us *veto*s (within the **(C)** set of cuts) one quark jet in these processes. Here one has also to account for a reaction where the Higgs boson is produced in association with the W - or Z -bosons decaying into quark pairs. In Fig. 2 Feynman diagrams for these subprocesses are shown. The W/Z fusion processes were calculated in [34, 35], while the processes of W/Z associated production were considered in [36]. In total the W/Z fusion and association rates are about 33-40% of the QCD signal channels for $M_H = 100-140$ GeV. Here we used $Q^2 = (M_V/2)^2$ as the parton factorization scale for the fusion processes (V denotes W or Z), and $Q^2 = (M_V + M_H)^2$ for the associated production.

Note that the process $pp \rightarrow H + t + \bar{t}$ can also contribute to the final state $\gamma\gamma + jet$. However, our preliminary estimate has shown that the corresponding rate is very small. So, to be conservative we do not take into account this signal channel in our analysis.

In total, we obtain 4.1-6.6 fb total cross section of the signal subprocesses in the Higgs mass range $M_H = 100-140$ GeV.

Let us now look at the irreducible background. As we already discussed in the previous section, the subprocess $gq \rightarrow \gamma + \gamma + q$ gives the main background. Another channel, $q\bar{q} \rightarrow \gamma + \gamma + g$, gives about 36% of the main gq contribution. Feynman diagrams of these subprocesses are shown in Fig. 3.

The one-loop background process $gg \rightarrow \gamma + \gamma + g$ exists, when the photons are radiated from the quark loop. Unfortunately this subprocess is not calculated yet. We estimate its cross section by means of PYTHIA 6.1 simulations. For this purpose one can initialize PYTHIA subprocess 114, $gg \rightarrow \gamma + \gamma$, and switch on gluon bremsstrahlung from the initial states. This is definitely only one of many other physical contributions to this process. The result of these simulations shows us that this background is about 2-4% of the overall contribution coming from the gq and $q\bar{q}$ channels.

In total, the irreducible background amounts to 10.9-19.3 fb/2GeV for the Higgs mass range under discussion ($M_H = 100 - 140$ GeV).

4.4 Reducible QCD background

In this section we discuss the results of PYTHIA 6.1 simulations for various QCD processes which could give a background due to radiation of photons from the fragmentating quarks or gluons. Note that the photon production mechanism is related in particular to a π^0 -meson (and other neutrals) production – the energetic π^0 's could result in a photon pair which will be detected as a single photon in the electromagnetic calorimeter. Thus, an important characteristic is the π^0/γ rejection factor of the calorimeter. For example, for CMS detector it is assumed [3] to be ~ 3 from the possibility to distinguish the two photon clusters. Nevertheless, we do not take into account this factor in our present analysis.

One kind of reducible background is coming from the subprocesses

$$gq \rightarrow \gamma + g + q, \quad gg \rightarrow \gamma + q + \bar{q}, \quad q\bar{q}' \rightarrow \gamma + q(g) + q'(g),$$

in the cases when the final gluon or quark produces an energetic photon and the jet escapes the detection. The corresponding rates were estimated by the following algorithm. For definiteness let us consider the subprocess $gq \rightarrow \gamma + g + q$. Firstly, we calculate its cross section by means of CompHEP imposing the kinematical cuts for a gluon the same as for a photon. We apply the set **(C)** of kinematical cuts on this 3-body final state and integrate in the invariant mass of photon and gluon (regarded as a photon) over the interval of 2 GeV around the central point $M_{\gamma\gamma} = M_H$. The cross section turns out to be $\sigma \sim 2$ pb ($\sigma' \sim 2.7$ pb when the final quark is considered as a photon). Then the probability to get a high energy (> 40 GeV) photon from the fragmentating quark or gluon without further generation of a detectable jet is estimated as $P(\gamma/q_{veto}) \sim 2 \cdot 10^{-4}$ and $P(\gamma/g_{veto}) \sim 0.3 \cdot 10^{-4}$ [39]. As a result we have an estimate of this background as $[\sigma \times P(\gamma/q_{veto}) + \sigma' \times P(\gamma/g_{veto})] \sim 1.1$ fb/2GeV. Corresponding contributions from the gg and $q\bar{q}'$ subprocesses are estimated in the same manner and the result is ~ 0.5 fb/2GeV for each channel. Altogether these channels give a background at the level of ~ 2.1 fb/2GeV.

Another kind of reducible background could come from the subprocesses

$$gq \rightarrow \gamma + q, \quad q\bar{q} \rightarrow \gamma + g,$$

when the second photon is produced during the quark or gluon fragmentation but this jet is still detected. Let us consider the gq channel. As a first step we evaluate with the help of CompHEP the cross section of this process, applying the $p_t > 40$ GeV, $|\eta_\gamma| < 2.5$ and $|\eta_q| < 2.5$ cuts, and it turns out to be of order of 2800 pb. For further PYTHIA simulations we switch on a fragmentation in this process and look for two photons (which can be, in particular, a photon plus π^0) satisfying the corresponding cuts from the set **(C)**. We require also that the invariant mass of this pair should be in the interval $90 < M_{\gamma\gamma} < 140$ GeV. In addition we require these photons to be separated: no charged particles in the cone $\Delta R < 0.3$ are produced and the total energy of neutral particles in the conical area $0.04 < \Delta R < 0.3$ is less than 2 GeV. Then we look at these events and try to find, with the help of the jet finder built in PYTHIA, a jet having proper E_t and separated from the generated ‘good’ photons. We generated in total more than $3 \cdot 10^6$ events and no good events were found. As a result we estimate this background to be ≤ 0.4 fb/2GeV. The analogous estimate for the channel $q\bar{q}$ is much smaller (≤ 0.01 fb/2GeV).

From this latter simulations one can extract a parameter which is useful for estimate of the next type of reducible background. The probability to get an energetic photon from the fragmentating 40 GeV jet, separated from each other so that the jet is still detectable, can be estimated at a level of $P(\gamma/jet_{det}) \sim 4 \cdot 10^{-4}$ [39]. So, this background from the subprocesses $gq \rightarrow \gamma + q$ can be estimated as $2800\text{pb} \times 4 \cdot 10^{-4} \times \hat{P}(\gamma, \gamma)$, where $\hat{P}(\gamma, \gamma)$ is the unknown probability for two photons (or the photon and π^0) to be separated and to have their invariant mass within the interval $M_H - 1\text{GeV} < M_{\gamma\gamma} < M_H + 1\text{GeV}$. From the above simulations one obtains $\hat{P}(\gamma, \gamma) \leq 4 \cdot 10^{-5}$.

Third kind of reducible background could comes from the pure QCD subprocesses of $2 \rightarrow 2$ type, when both particles in the final state are gluons or quarks. We have to discuss these processes in connection with the probability to get two separated and energetic photons from the fragmentating quarks and gluons. There are possible contributions from the following subprocesses⁵

$$gg \rightarrow g(q) + g(\bar{q}), \quad gq \rightarrow g + q, \quad qq' \rightarrow q(g) + q'(g).$$

We estimate the corresponding rates by the following formula

$$\sigma \times P\left(\frac{\gamma}{jet_{det}}\right) \times P\left(\frac{\gamma}{jet'_{veto}}\right) \times \hat{P}(\gamma, \gamma).$$

Here σ stands for the cross section of the subprocess when the cuts $p_t > 40$ GeV and $|\eta_{jet}| < 2.5$ are applied. For the gg channel $\sigma = 1.3 \cdot 10^7$ pb. However, this enormous cross section is reduced to the insignificant level of $\leq 1.4 \cdot 10^{-3}$ fb by probabilities to get the proper photons. For other channels σ has values much smaller and we have rates of $\leq 10^{-3}$ fb for the gq and of $\leq 10^{-4}$ fb for the qq' ones. In total, this type of background gives a very small contribution of ~ 0.0025 fb/2GeV.

Finally we consider reactions of the $2 \rightarrow 3$ type when all three particles in the final state are gluons or quarks. At the parton level these processes can be derived from the processes discussed in the previous paragraph taking into account gluon radiation. So, as in the previous case, there are three subgroups of such processes with the gg , gq and qq' initial states. Here we have to account for events where two separated and energetic photons are produced by fragmentating quarks or gluons which escape detection. Let us consider the subprocess $gg \rightarrow g + g + g$. If we consider two of final gluons as photons and apply our basic set **(C)** of kinematical cuts the cross section is of order of $5.8 \cdot 10^3$ pb/2GeV. To get the necessary estimate we use the formula

$$\sigma \times P\left(\frac{\gamma}{jet_{veto}}\right) \times P\left(\frac{\gamma}{jet'_{veto}}\right).$$

In the gg case we have to multiply this formula by a combinatorial factor 3 due to three variants to produce two photons from different gluons. We neglect the possibility when two photons are produced from the same gluon jet while the other gluon jet escapes detection. So, this background is estimated at the level of ~ 0.016 fb/2GeV. The analogous estimates for other subprocesses of this type give 0.018

⁵Note that there is some double counting for the first type of QCD reducible background analysed in the beginning of this section due to the photon radiation from the final quarks. We neglect this double counting in our rather rough estimates. The same remark is valid for the last type of the QCD background discussed in this section.

$\text{fb}/2\text{GeV}$ for gq and $0.002 \text{ fb}/2\text{GeV}$ for the qq' channels. In total, this type of QCD background gives rather small contribution of $\sim 0.036 \text{ fb}/2\text{GeV}$.

Altogether four types of QCD reducible background processes contribute with a rate of $\leq 2.2 \text{ fb}/2\text{GeV}$. This is not a negligible background and one has to take it into account analysing the reaction $pp \rightarrow \gamma\gamma + \text{jet}$.

Now we can conclude that the QCD reducible background, connected with the probability to get a photon from the fragmentating gluons or quarks, is potentially dangerous, especially if we remember various uncertainties in our estimates. Nevertheless, this background turns out to be less than 20% of the irreducible background.

4.5 Summary

From Table 2 one can see, first of all, that with an integrated luminosity of 10 fb^{-1} this channel can give 40-70 signal events with a number of background events only by a factor of 2-3 higher. This result was obtained for the basic set of kinematical cuts (**C**) (see Section 4.2) and for resolution determined mass interval $M_H \pm 1 \text{ GeV}$ in the two-photon invariant mass $M_{\gamma\gamma}$. The significances are $N_S/\sqrt{N_B} \sim 4.0, 5.3$ and 4.1 for $M_H = 100, 120$ and 140 GeV , respectively, showing good prospects for discovery of the light Higgs boson in this reaction at low LHC luminosity, when total statistics collected is $\sim 30 \text{ fb}^{-1}$. These results also mean that each year of LHC operation at high luminosity of $10^{34} \text{ cm}^{-2} \text{s}^{-1}$ will give hundreds of events with high p_t Higgs bosons associated with high p_t jet in central detector. The signal significance will be of order of 15 in this case.

Most important advantage of the reaction $pp \rightarrow \gamma\gamma + \text{jet}$ in comparison with the 'standard' channel $pp \rightarrow \gamma\gamma$ is significant improvement of the *Signal/Background* ratio. Let us remind that in $pp \rightarrow \gamma\gamma$ this ratio is $\sim 1/15$ (calculated in the LO approximation and with 2 GeV photon invariant mass interval for the background, as in our case). For the reaction $pp \rightarrow \gamma\gamma + \text{jet}$ the *Signal/Background* ratio is $\sim 1/2 - 1/3$. Signal significance $N_S/\sqrt{N_B}$ is the same for both channels.

However, we should stress that in present analysis we did not account for various factors which can change the Higgs significance considerably. Let us review these factors and start from those which should help to improve the values obtained for the Higgs signal significance.

First, the results presented in Table 2 for hard subprocesses have been obtained in leading orders α_s^3 for the QCD signal processes and α_s for the background. As we have mentioned in Section 4.1 the next-to-leading QCD corrections are unknown for these subprocesses.⁶ Notice that the NLO corrections to the hard subprocesses in the $pp \rightarrow \gamma\gamma + X$ inclusive reaction increase the Higgs production cross section by about 60% (see [27] and the references therein). Of course, it is very probable that the NLO corrections enhance somehow the rates of background processes as well. However, due to a lower strong coupling order of the background processes one can assume their QCD corrections to be smaller than for the signal.

There are possible ways to improve the significance of the $\gamma\gamma + \text{jet}$ channel by applying weaker jet cuts. In particular, if the detection of jet is possible at large rapidities, up to $|\eta_{\text{jet}}| \sim 4$ (involving the very forward hadron calorimeter), the significance will increase by $\sim 14\%$. Furthermore, if the determination of jet is reliable with $E_t^{\text{jet}} > 30 \text{ GeV}$ then the significance will increase by $\sim 8\%$ in comparison with the case of basic kinematical cuts (**C**).

Let us remember now that for the CMS PbWO₄ electromagnetic calorimeter the two-photon invariant mass resolution is expected to be significantly better than 1 GeV in low luminosity running. For example, in [3] the following two-photon mass resolutions were considered for the reaction $pp \rightarrow \gamma\gamma + X$ at low luminosity: $\sigma_m^L = 540$ and 600 MeV for $M_H = 110$ and 130 GeV , respectively. Surely, in this case the Higgs significance will increase noticeably compared to the estimates made earlier in this paper.

However, there are also many factors reducing signal significance. One of them is that the one-loop subprocess $gg \rightarrow \gamma + \gamma + g$ contributing to the background, unfortunately, is not still calculated – its exact matrix element is unknown. Our estimate of its rate is rather small, $\sim 0.2\text{-}0.8 \text{ fb}/2\text{GeV}$. However, these numbers have been obtained by means of PYTHIA simulations for the process $gg \rightarrow \gamma + \gamma$ where the final gluon is radiating from the initial state only. We expect the rate of this background to be higher due to other mechanisms of the final gluon radiation.

⁶Some progress has appeared recently for the signal, see Ref. [37].

Furthermore, the reducible QCD background is potentially dangerous as a rule at hadron colliders. We have estimated this background at the level of $\leq 2.2 \text{ fb}/2\text{GeV}$. Of course, more accurate evaluation of this background would be desirable taking into account the detailed simulation of the ATLAS and CMS detectors. Due to this discussion one can remember that similar analysis for the inclusive $pp \rightarrow \gamma\gamma + X$ reaction showed [3, 4] that the reducible QCD background can be suppressed at the level of $< 10\%$ of the irreducible bias.

The efficiency of photons detection was not taken into account in our estimates. In our case the photons have large transverse momenta $p_t^\gamma > 40 \text{ GeV}$ and radiated with small rapidities $|\eta_\gamma| < 2.5$. So one can hope that the photon detection efficiency will be high enough. At present time for both ATLAS and CMS detectors this efficiency is estimated at the level ≈ 0.8 . Experimental efficiency of hard jet detection was also not taken into account.

Finally, combining all these factors one can hope that they could at least compensate each other, and our general conclusion about a possibility to discover the light Higgs boson during the LHC operation at low luminosity is still kept.

Conclusions

The channel $\gamma\gamma + jet$ gives very promising discovery possibilities for the Higgs boson with a mass of 100-140 GeV during the LHC operation at low luminosity of $\sim 10^{33} \text{ cm}^{-2} \text{ s}^{-1}$. With an integrated luminosity of 30 fb^{-1} 120-200 signal events could be observed with 330-600 background events per 2 GeV interval of two photon invariant mass, showing a signal significance of $\sim 7 - 8.5$. For high LHC luminosity of $10^{34} \text{ cm}^{-2} \text{ s}^{-1}$ hundreds of Higgs bosons will be observed with a significance of order of 15 for one year data accumulation. The reducible QCD background is at the level of $\leq 20\%$ of the irreducible one. The next-to-leading QCD corrections, not calculated at present time, could enhance the signal more than the background. Higher two-photon invariant mass resolution that is now under discussion for the CMS PbWO₄ calorimeter (see [3], $\sigma_m^L \sim 500 - 600 \text{ MeV}$ at $M_H = 110 - 130 \text{ GeV}$) could increase highly the significance of signal. On the other hand, the efficiencies of photon and jet detection that we did not take into account decrease the signal significance. These factors (as well as others discussed above) work in the opposite directions and it is probable that they compensate each other.

Acknowledgements

We are grateful to D. Denegri and N. Stepanov for attracting our attention to the signatures with high p_t jets. We thank very much them and S. Abdullin for the fruitful collaboration as well as E. Boos, M. Mangano and A. Pukhov for many useful discussions. We are grateful to D. Kovalenko for his collaboration in implementing the loop vertices in CompHEP. Our simulations by PYTHIA would have been impossible without the help of S. Abdullin and N. Stepanov. We are also indebted to them and I. Goloutvine, A. Nikitenko and R. Kinnunen for the interesting discussions about the CMS detector.

Our participation in the CMS Collaboration has been realized due to the kind promotion of V. Matveev and I. Goloutvine and the support of the Russian Ministry of Science and Technologies. This work was partially supported also by the European Association INTAS (grant 93-1180ext) and the Russian Foundation for Basic Research (grants 96-02-18635 and 96-02-19773).

We express our sincere gratitude to the CMS Collaboration and the CERN PPE Division for the hospitality and kind assistance during our stay at CERN.

References

- [1] M.N. Dubinin, V.A. Ilyin and V.I. Savrin, CMS NOTE 97/101, December 5, 1997.
- [2] *Proc.of the Aachen Workshop on Large Hadron Collider*, ed. G. Jarlskog and D. Rein, CERN report 90-10, vol.II, 1990.
- [3] CMS Technical Proposal, CERN/LHCC report 94-38, 1994.
- [4] ATLAS Calorimeter Performance, Technical Design Report 1, CERN/LHCC 96-40, December 1996.

- [5] R.K. Ellis, I. Hinchliffe, M. Soldate and J.J. van der Bij, Nucl. Phys. **B297** (1988) 221.
- [6] C. Kao, Phys. Lett. **B328** (1994) 420.
- [7] R.A. Alanakyan and V.H. Grabski, hep-ph/9711436.
- [8] U. Baur and F.W.N. Glover, Nucl. Phys. **B339** (1990) 38.
- [9] D. Rainwater and D. Zeppenfeld, Preprint MADPH-97-1023, December 1997, hep-ph/9712271.
- [10] S. Abdullin, A. Knezevic, R. Kinnunen and N. Stepanov, CMS TN/94-247, 1994.
- [11] T. Sjostrand, Comp. Phys. Comm. **82** (1994) 74.
- [12] P.A. Baikov et al., in: *Proc. of X Workshop QFTHEP-95*, ed. B. Levchenko and V. Savrin, Moscow, 1996, p.101, hep-ph/9701412.
E.E. Boos, M.N. Dubinin, V.A. Ilyin, A.E. Pukhov and V.I. Savrin, Preprint INP MSU 94-36/358, SNUCTP 94-116, 1994, hep-ph/9503280.
- [13] V.A. Ilyin, D.N. Kovalenko and A.E. Pukhov, Int. J. Mod. Phys. **C6** (1996) 761.
D.N. Kovalenko and A.E. Pukhov, Nucl. Instrum. and Methods **389** (1997) 299.
- [14] G.P. Lepage, J. Comp. Phys. **27** (1978) 192; Cornell preprint CLNS-80/447, 1980.
- [15] H.L. Lai et al. (CTEQ collaboration), Phys. Rev. **D51** (1995) 4763.
- [16] H.L. Lai et al. (CTEQ collaboration), Phys. Rev. **D55** (1997) 1280.
- [17] A.D. Martin, R.G. Roberts and W.J. Stirling, Phys. Lett. **B354** (1995) 155.
- [18] M. Gluck, E. Reya, A. Vogt, Z.Phys. **C53** (1992) 127.
- [19] M. Spira, DESY T-95-05, hep-ph/9510347.
A. Djouadi, J. Kalinowski and M. Spira, DESY 97-079, hep-ph/9704448.
M. Spira, Nucl. Instrum. and Methods **389** (1997) 357.
- [20] *Review of Particle Physics*, Part I, Phys. Rev. **D54** (1996) N1.
- [21] A. Yagil, Plenary talk in: *Europhysics Conference on High Energy Physics* (August 19-26, 1997, Jerusalem).
- [22] S.G. Gorishny, A.L. Kataev, S.A. Larin and L.R. Surguladze, Mod. Phys. Lett. **A5** (1990) 2703.
N. Gray, D.J. Broadhurst, W. Grafe and K. Schilcher, Z. Phys. **C48** (1990) 673.
A.L. Kataev and V.T. Kim, Mod. Phys. Lett. **A9** (1994) 1309.
- [23] J. Fleischer and F. Jegerlehner, Phys. Rev. **D23** (1981) 2001.
D.Yu. Bardin, B.M. Vilenski and P.Kh. Khristova, Sov. J. Nucl. Phys. **53** (1991) 152.
A. Dabelstein and W. Holllik, Z. Phys. **C53** (1992) 507.
B.A. Kniehl, Nucl. Phys. **B376** (1992) 3.
- [24] J. Ellis, M.K. Gaillard and D.V. Nanopoulos, Nucl. Phys. **B106** (1976) 292.
A.I. Vainshtein, M.B. Voloshin, V.I. Zakharov and M.A. Shifman, Sov. J. Nucl. Phys. **30** (1979) 711.
E. Eichten, I. Hinchliffe, K. Lane and C. Quigg, Rev. Mod. Phys. **56** (1984) 579; Rev. Mod. Phys. **58** (1985) 1065.
L.B. Okun, *Leptons and Quarks*, North Holland, 1984.
- [25] S. Dawson, Nucl. Phys. **B359** (1991) 283.
- [26] A. Djouadi, M. Spira and P.M. Zerwas, Phys. Lett. **B264** (1991) 440.

- [27] M. Spira, A. Djouadi, D. Graudenz and P.M. Zerwas, Nucl. Phys. **B453** (1995) 17.
- [28] K.G. Chetyrkin, B.A. Kniehl and M. Steinhauser, Phys. Rev. Lett. **79** (1997) 353.
- [29] A. Djouadi and P. Gambino, Phys. Rev. Lett. **73** (1994) 2528.
Y. Liao and X. Li, hep-ph/9605310.
- [30] H1 collaboration, S. Aid et al., Nucl. Phys. **B439** (1995) 471; **B470** (1996) 3.
ZEUS collaboration, M. Derrick et al., Z. Phys. **C65** (1995) 379; Report DESY-96076, 1996.
- [31] T.G. Rizzo, Phys. Rev **D22** (1980) 722.
W.-Y. Keung and W.J. Marchiano, Phys. Rev **D30** (1984) 248.
- [32] V.A. Ilyin, D.N. Kovalenko and V.I. Savrin, in preparation.
- [33] V. Del Duca and C.R. Schmidt, Phys. Rev. **D49** (1994) 177.
- [34] S. Dawson, Nucl. Phys. **B249** (1984) 42.
- [35] G.L. Kane, W.W. Repko and W.B. Rolnick, Phys. Lett. **B148** (1984) 367.
- [36] J. Gunion, G. Kane and J. Wudka, Nucl. Phys. **B299** (1988) 231.
P. Agrawal and S.D. Ellis, Phys. Lett. **B229** (1989) 145.
- [37] C.R. Schmidt, MSUHEP-70723, July 1997, hep-ph/9707448.
- [38] S. Abdullin, A. Khanov and N. Stepanov, *CMSJET*, CMS TN/94-170, 1994.
- [39] S. Abdullin, private communication

Tables

a)

		HB		HF			VF			
$ \eta^j <$		1.00	1.50	2.00	2.40	3.00	3.50	4.00	4.50	5.00
σ	S	2.16	3.10	3.84	4.32	4.79	5.01	5.12	5.14	5.16
fb	B / 2 GeV	6.48	9.16	11.04	11.89	12.64	12.76	12.80	12.80	12.82
	$\frac{\sigma_S}{\sqrt{\sigma_B}}$	0.85	1.03	1.15	1.25	1.35	1.40	1.43	1.44	1.44
$\frac{\sigma_S}{\sigma_B}$		0.33	0.34	0.35	0.36	0.38	0.39	0.40	0.40	0.41

b)

$E_t^{jet} >$ GeV		20	25	30	35	40	45	50
σ	S	9.25	7.43	6.05	5.07	4.32	3.73	3.27
	B / 2 GeV	30.86	24.72	19.62	15.32	11.89	9.22	7.24
$\frac{\sigma_S}{\sqrt{\sigma_B}}$		1.66	1.49	1.36	1.29	1.25	1.23	1.22
$\frac{\sigma_S}{\sigma_B}$		0.30	0.30	0.31	0.33	0.36	0.41	0.45

Table 1: Cross sections of the main signal (**S**) and background (**B**) processes $pp \rightarrow H + g \rightarrow \gamma\gamma + g$ and $pp \rightarrow \gamma + \gamma + q$, as a function of the jet a) rapidity cuts and b) transverse energy. The basic set (**C**) of cuts is imposed on other variables. $M_H = 120$ GeV. PDF set CTEQ4m is used. All subprocesses are evaluated in QCD leading order and the 2nd order running α_s with normalization $\alpha_s(M_Z) = 0.118$. $Q^2 = M_H^2 + 2(E_t^{jet})^2$ is taken as the QCD scale for running α_s and as the parton factorization scale. The $\gamma\gamma$ invariant mass for the background is integrated over the range $M_H - \Delta M_{\gamma\gamma} < M_{\gamma\gamma} < M_H + \Delta M_{\gamma\gamma}$ with $\Delta M_{\gamma\gamma} = 1$ GeV.

	Hard subprocess	σ, fb		
		$M_H = 100 \text{ GeV}$	120 GeV	140 GeV
S	$gg \rightarrow H + g$	2.55	4.32	3.75
	$gq \rightarrow H + q$	0.39	0.59	0.50
	$q\bar{q} \rightarrow H + g$	0.006	0.007	0.006
S ($jet_{det} + jet_{veto}$)	$qq' \rightarrow H + q + q'$	0.88	1.33	1.16
	$q\bar{q}' \rightarrow H + W$	0.25	0.31	0.19
	$q\bar{q} \rightarrow H + Z$	0.071	0.087	0.054
B / 2 GeV	$gq \rightarrow \gamma + \gamma + q$	7.83	11.89	14.86
	$q\bar{q} \rightarrow \gamma + \gamma + g$	2.84	3.50	3.64
	$gg \rightarrow \gamma + \gamma + g$ (*)	~ 0.2	~ 0.5	~ 0.8
B / 2 GeV ($\frac{\gamma}{jet_{veto}}$)	$gq \rightarrow \gamma + g + q$ (*)		~ 1.1	
	$gg \rightarrow \gamma + q + \bar{q}$ (*)		~ 0.5	
	$qq' \rightarrow \gamma + q + q'$		~ 0.5	
B / 2 GeV ($\frac{\gamma}{jet_{det}}$)	$gq \rightarrow \gamma + q$ (*)		≤ 0.4	
	$q\bar{q} \rightarrow \gamma + g$ (*)		≤ 0.001	
B / 2 GeV ($\frac{\gamma}{jet_{det}} + \frac{\gamma}{jet_{veto}}$)	$gg \rightarrow g + g$ (*)		≤ 0.0014	
	$gq \rightarrow g + q$ (*)		≤ 0.001	
	$qq' \rightarrow q + q'$ (*)		$\ll 0.001$	
B / 2 GeV ($\frac{\gamma}{jet_{veto}} + \frac{\gamma}{jet_{det}}$)	$gg \rightarrow g + g + g$ (*)		~ 0.016	
	$gq \rightarrow g + g + q$ (*)		~ 0.018	
	$qq' \rightarrow g + jet + jet'$ (*)		~ 0.002	

Table 2: Summary for the $pp \rightarrow \gamma\gamma + jet$ reaction. Contributions of different subprocesses are shown for the basic set of kinematical cuts (**C**) (see Section 4.2). PDF set CTEQ4m is used. All subprocesses are evaluated in QCD leading order and the 2nd order running α_s with normalization $\alpha_s(M_Z) = 0.118$. $Q^2 = M_H^2 + 2(E_t^{jet})^2$ was taken as the QCD scale for running α_s and as the parton factorization scale in hard QCD subprocesses. The values $Q^2 = (M_V/2)^2$ and $Q^2 = (M_V + M_H)^2$, where $V = (W, Z)$, are used for the parton factorization scale in the W/Z fusion and W/Z associated Higgs signal processes, correspondingly. The $\gamma\gamma$ invariant mass for the background is integrated over the range $M_H - \Delta M_{\gamma\gamma} < M_{\gamma\gamma} < M_H + \Delta M_{\gamma\gamma}$ with $\Delta M_{\gamma\gamma} = 1 \text{ GeV}$. Asterisk '*' marks the results of the PYTHIA 6.1 simulations. Other results are obtained with the help of CompHEP package.

Figures

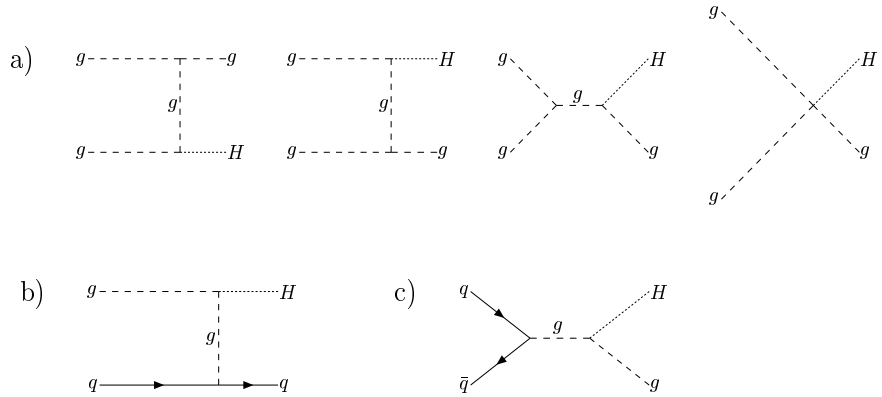


Figure 1: Feynman diagrams for the QCD signal subprocesses: a) $gg \rightarrow H + g$, b) $gg \rightarrow H + q$ and c) $q\bar{q} \rightarrow H + g$. In SM the ggH and $gggH$ vertices include quark loops. In the effective Lagrangian approximation (1,2) these vertices are point-like with the coupling constant λ_{ggH} .

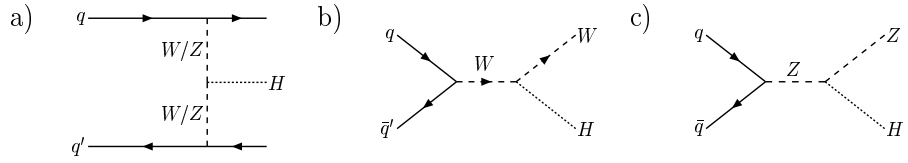


Figure 2: Feynman diagrams for the signal subprocesses with a) WW and ZW fusion mechanisms of the Higgs boson production, b) associated W -boson and c) associated Z -boson production.

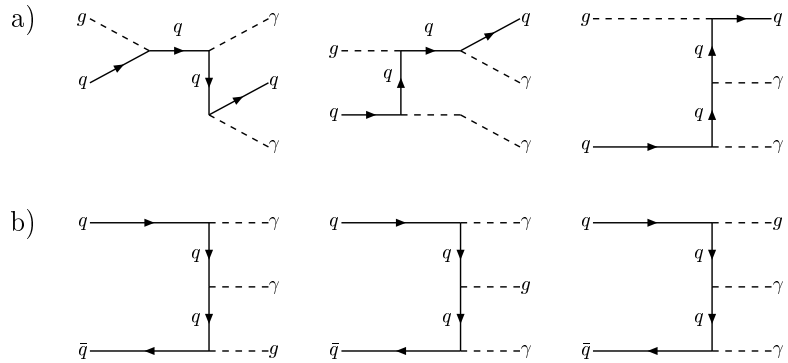


Figure 3: Feynman diagrams for the subprocesses a) $gq \rightarrow \gamma + \gamma + q$ and b) $q\bar{q} \rightarrow \gamma + \gamma + g$ contributing to the background.

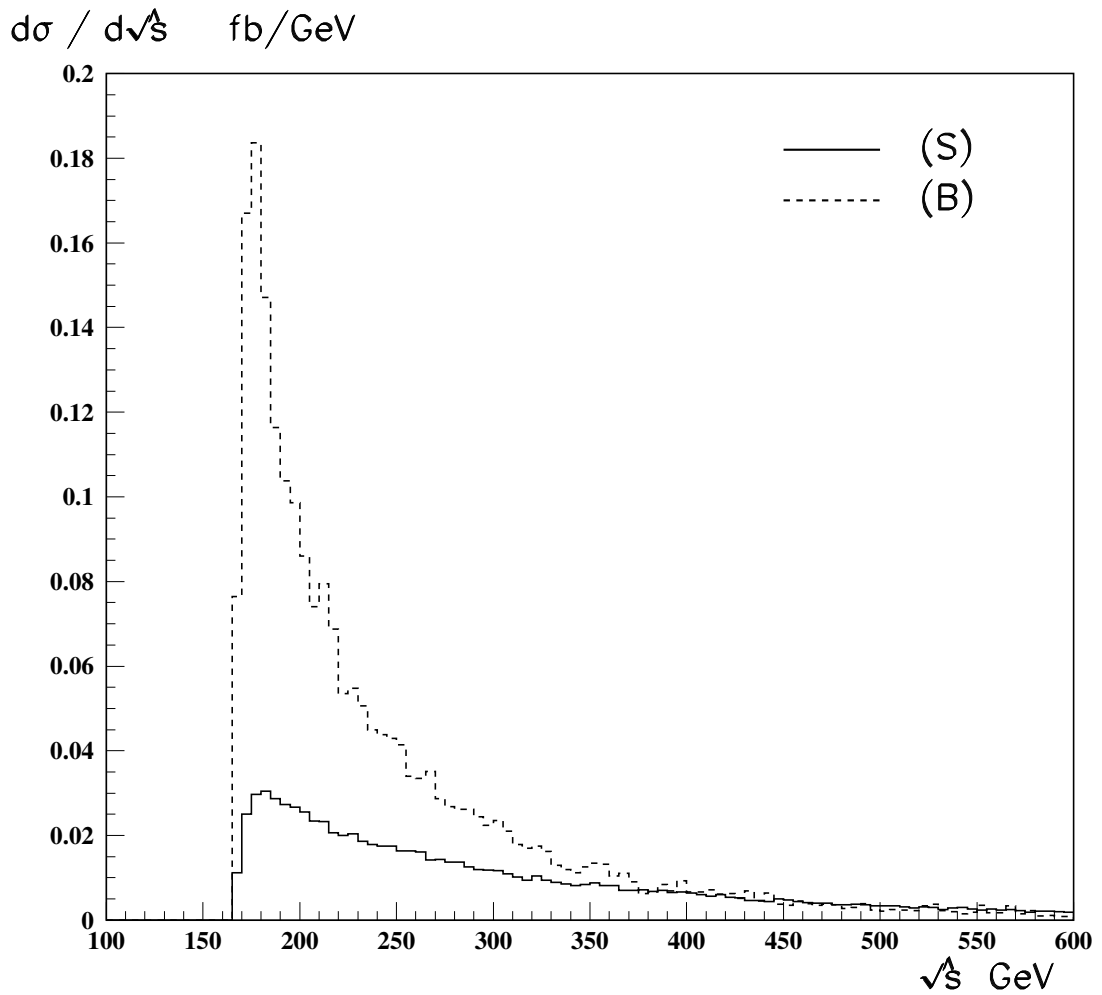


Figure 4: Distributions in the parton c.m. energy $\sqrt{\hat{s}}$ for the main signal (S) and background (B) processes $pp \rightarrow H + g \rightarrow \gamma\gamma + g$ and $pp \rightarrow \gamma + \gamma + q$. Energy $\sqrt{s} = 14$ TeV and the Higgs boson mass $M_H = 120$ GeV. CTEQ4m PDF set and $Q^2 = M_H^2 + 2(E_t^{jet})^2$ are used. The basic set of kinematical cuts (C) is imposed. The $\gamma\gamma$ invariant mass for the background is integrated over the range $M_H - \Delta M_{\gamma\gamma} < M_{\gamma\gamma} < M_H + \Delta M_{\gamma\gamma}$ with $\Delta M_{\gamma\gamma} = 1$ GeV.

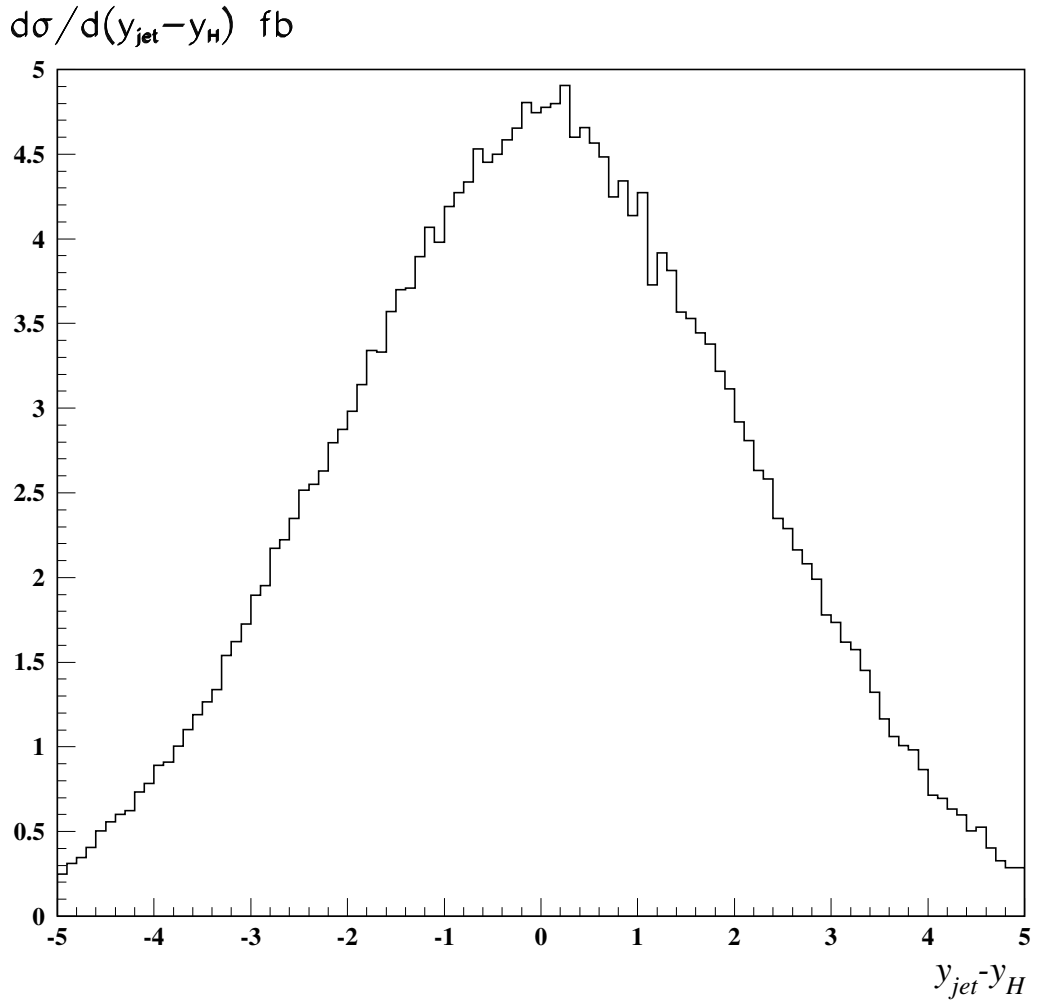


Figure 5: Distribution in rapidity interval $y_{jet} - y_H$ for the main signal (S) process $pp \rightarrow H + g \rightarrow \gamma\gamma + g$. Energy $\sqrt{s} = 14$ TeV and the Higgs boson mass $M_H = 120$ GeV. CTEQ4m PDF set and $Q^2 = M_H^2 + 2(E_t^{jet})^2$ are used. The basic set of kinematical cuts (C) is imposed.

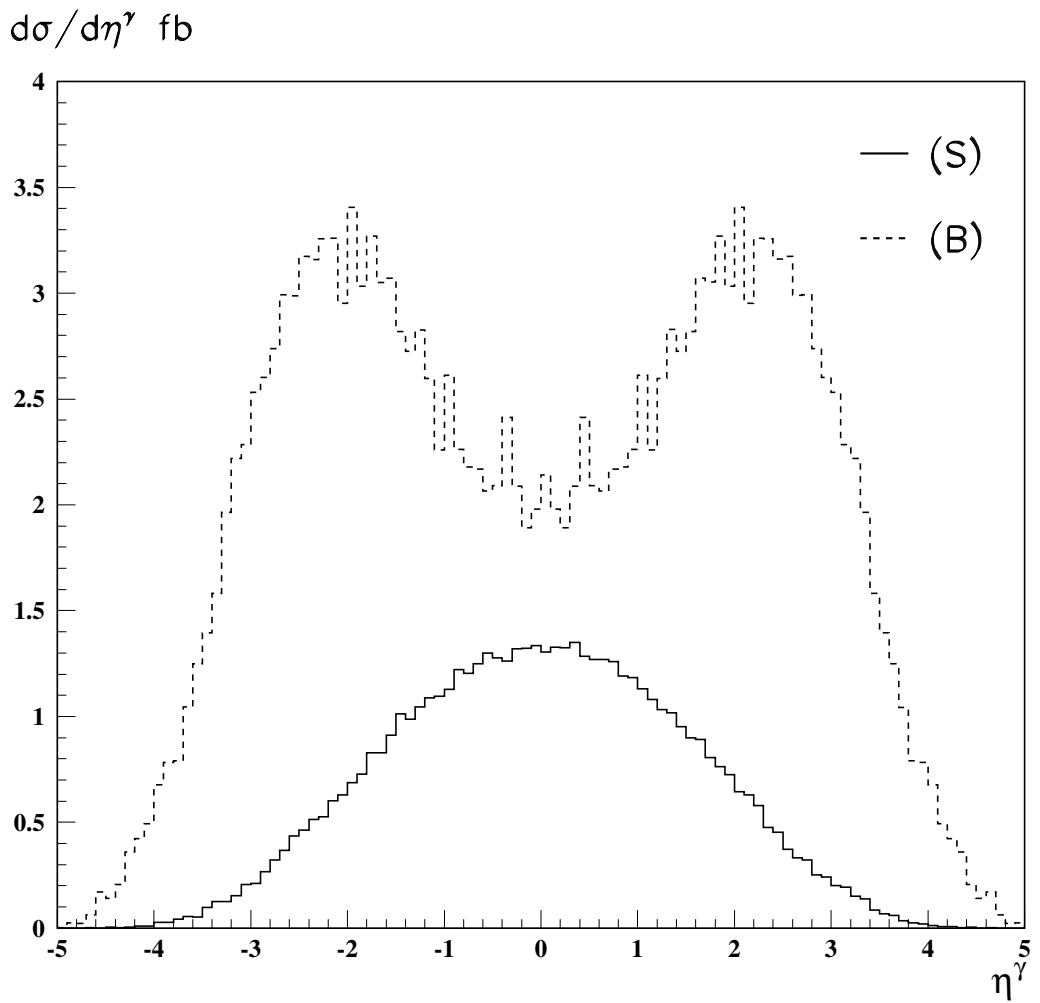


Figure 6: Distributions in photon rapidity for the main signal (S) and background (B) processes $pp \rightarrow H + g \rightarrow \gamma\gamma + g$ and $pp \rightarrow \gamma + \gamma + q$. Energy $\sqrt{s} = 14$ TeV and the Higgs boson mass $M_H = 120$ GeV. CTEQ4m PDF set and $Q^2 = M_H^2 + 2(E_t^{jet})^2$ are used. The basic set of kinematical cuts (**C**) is imposed on other variables. The $\gamma\gamma$ invariant mass for the background is integrated over the range $M_H - \Delta M_{\gamma\gamma} < M_{\gamma\gamma} < M_H + \Delta M_{\gamma\gamma}$ with $\Delta M_{\gamma\gamma} = 1$ GeV.

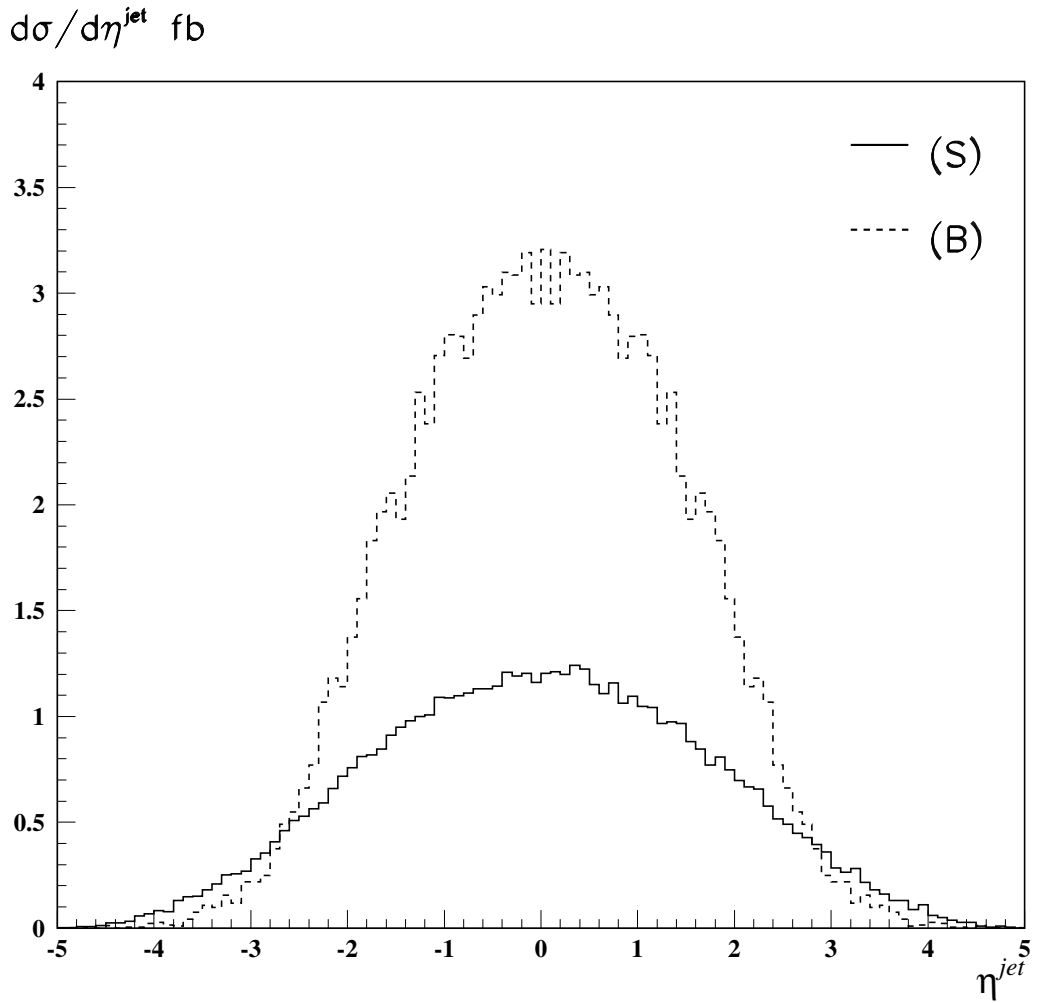


Figure 7: Distributions in jet rapidity for the main signal (S) and background (B) processes $pp \rightarrow H + g \rightarrow \gamma\gamma + g$ and $pp \rightarrow \gamma + \gamma + q$. Energy $\sqrt{s} = 14$ TeV and the Higgs boson mass $M_H = 120$ GeV. CTEQ4m PDF set and $Q^2 = M_H^2 + 2(E_t^{jet})^2$ are used. The basic set of kinematical cuts (**C**) was imposed on other variables. The $\gamma\gamma$ invariant mass for the background is integrated over the range $M_H - \Delta M_{\gamma\gamma} < M_{\gamma\gamma} < M_H + \Delta M_{\gamma\gamma}$ with $\Delta M_{\gamma\gamma} = 1$ GeV.

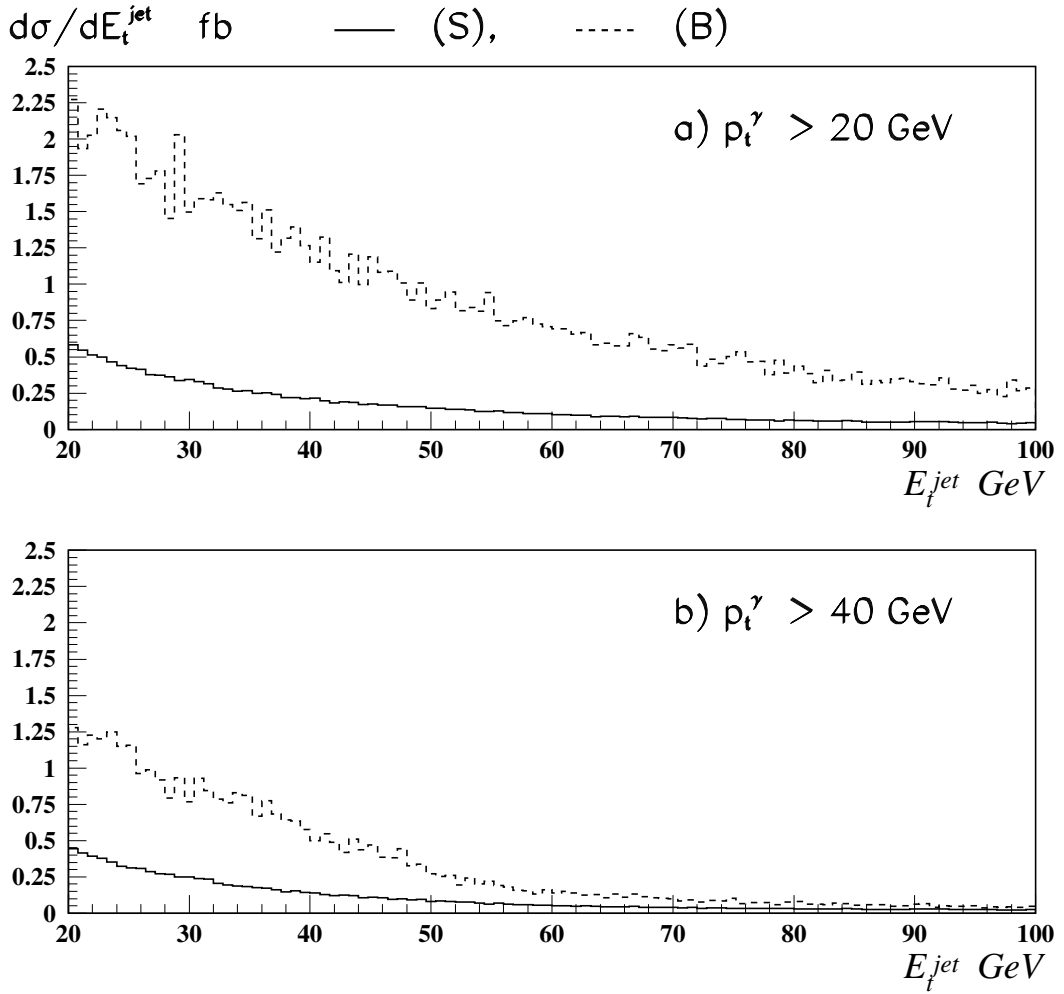


Figure 8: Distributions in jet transverse energy for the main signal (S) and background (B) processes $pp \rightarrow H + g \rightarrow \gamma\gamma + g$ and $pp \rightarrow \gamma + \gamma + q$. Energy $\sqrt{s} = 14$ TeV and the Higgs boson mass $M_H = 120$ GeV. CTEQ4m PDF set and $Q^2 = M_H^2 + 2(E_t^{jet})^2$ are used. The basic set of kinematical cuts (**C**) is imposed on other variables. The $\gamma\gamma$ invariant mass for the background is integrated over the range $M_H - \Delta M_{\gamma\gamma} < M_{\gamma\gamma} < M_H + \Delta M_{\gamma\gamma}$ with $\Delta M_{\gamma\gamma} = 1$ GeV.

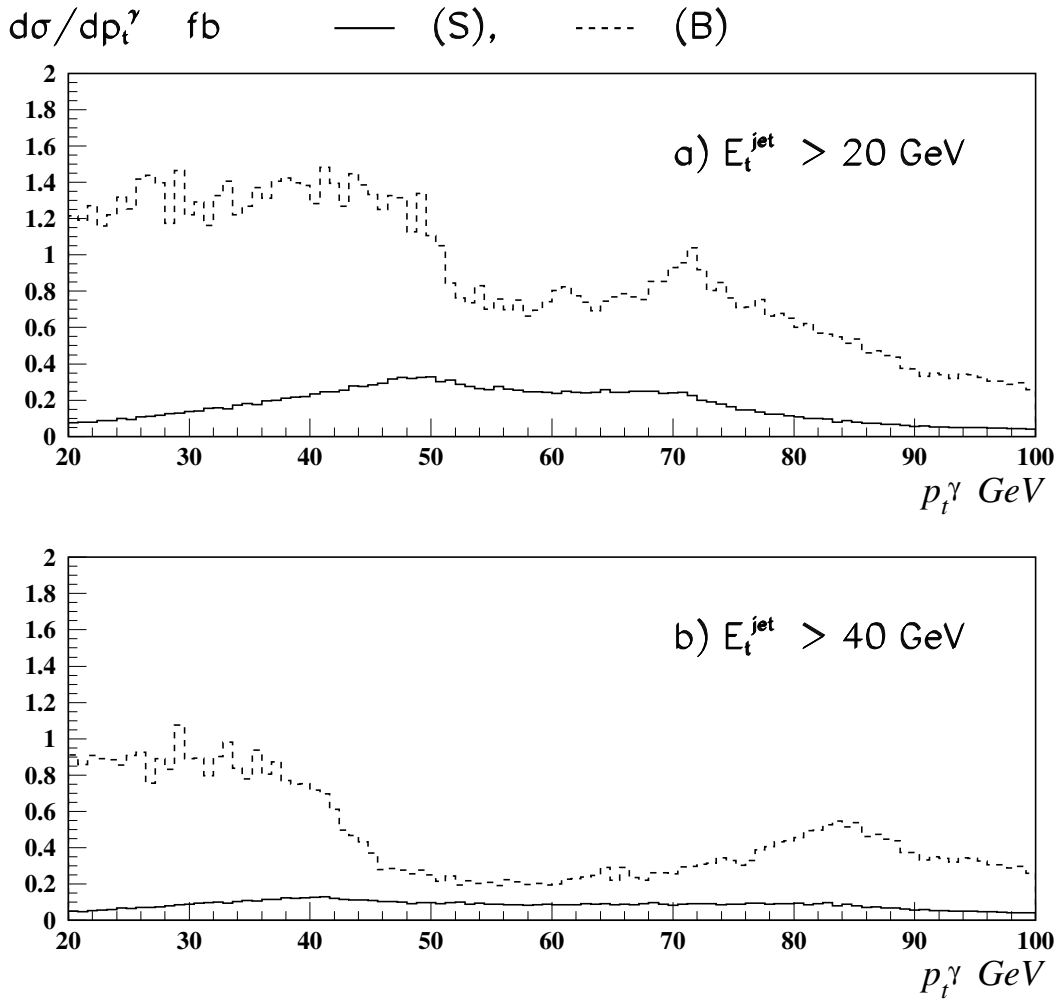


Figure 9: Distributions in photon transverse momentum for the main signal (S) and background (B) processes $pp \rightarrow H + g \rightarrow \gamma\gamma + g$ and $pp \rightarrow \gamma + \gamma + q$. Energy $\sqrt{s} = 14 \text{ TeV}$ and the Higgs boson mass $M_H = 120 \text{ GeV}$. CTEQ4m PDF set and $Q^2 = M_H^2 + 2(E_t^{\text{jet}})^2$ are used. The basic set of kinematical cuts (C) is imposed on other variables. The $\gamma\gamma$ invariant mass for the background is integrated over the range $M_H - \Delta M_{\gamma\gamma} < M_{\gamma\gamma} < M_H + \Delta M_{\gamma\gamma}$ with $\Delta M_{\gamma\gamma} = 1 \text{ GeV}$.